Published in final edited form as:
Cancer Res. 2012 October 15; 72(20): 5165–5173. doi:10.1158/0008-5472.CAN-12-0468.

RALBP1/RLIP76 depletion in mice suppresses tumor growth by inhibiting tumor neovascularization

Seunghyung Lee[1], **Jeremy G.T. Wurtzel**[1], **Sharad S. Singhal**[2], **Sanjay Awasthi**[2], and **Lawrence E. Goldfinger**[1]

[1]Department of Anatomy & Cell Biology and The Sol Sherry Thrombosis Research Center, Temple University School of Medicine, 3400 N. Broad Street, OMS 415, Philadelphia, PA 19140

[2]Department of Diabetes and Metabolic Diseases Research, Division of Diabetes, Endocrinology & Metabolism, Beckman Research Institute, City of Hope, National Medical Center, Duarte, CA 91010

Abstract

RalBP1/RLIP76 is a widely expressed multifunctional protein that binds the Ral and R-Ras small GTPases. In the mouse, RLIP76 is non-essential but its depletion or blockade promotes tumorigenesis and heightens the sensitivity of normal and tumor cells to radiation and cytotoxic drugs. However, its pathobiological functions which support tumorigenesis are not well understood. Here we show that RLIP76 is required for angiogenesis and for efficient neovascularization of primary solid tumors. Tumor growth from implanted melanoma or carcinoma cells was blunted in RLIP76$^{-/-}$ mice. An X-ray microCT-based method to model tumor vascular structures revealed defects in both the extent and form of tumor angiogenesis in RLIP76$^{-/-}$ mice. Specifically, tumor vascular volumes were diminished and vessels were fewer in number, shorter, and narrower in RLIP76$^{-/-}$ mice than in wild-type mice. Moreover, we found that angiogenesis was blunted in mutant mice in the absence of tumor cells, with endothelial cells isolated from these animals exhibiting defects in migration, proliferation and cord formation *in vitro*. Taken together, our results establish that RLIP76 is required for efficient endothelial cell function and angiogenesis in solid tumors.

Keywords

RalBP1/RLIP76; Tumor angiogenesis; Endothelial cell; Migration; X-ray micro-computed tomography

Introduction

Angiogenesis – the outgrowth of new blood vessels from existing ones, is required for progression of pathologies such as tumor growth and metastasis. Solid tumors require a nutrient blood supply to grow beyond ~1 mm diameter, and inhibiting tumor angiogenesis has long been pursued as an approach to preventing tumor growth and subsequent metastasis(1). Therefore it is important to identify specific modulators of tumor angiogenesis for therapeutic intervention in cancer. Angiogenesis is a complex process resulting from combined up-regulation of proliferation and migration in endothelial cells, driven by responses of these cells to angiogenic stimulants such as vascular endothelial

Correspondence should be addressed to: Lawrence Goldfinger - goldfinger@temple.edu. phone: 215.707.8157. fax: 215.707.2783.

Disclosure of Potential Conflicts of Interest
The authors declare that there are no potential conflicts of interest.

growth factor (VEGF). Endothelial cells are specialized squamous epithelia that form the inner core of all blood vessels, and are the sole cellular components of the microvasculature (capillaries). During initial stages of angiogenesis, proliferating and migrating endothelial cells convert to a spindle-shaped morphology and organize into branched capillary networks, which ultimately differentiate into fully-formed lumenal vessels carrying blood from the source vasculature to the new sites such as into solid tumors(1). These processes are regulated by complex cellular signaling networks(2).

Molecular controllers of angiogenic signaling networks are logical targets for therapeutic intervention. RLIP76 (Ral-interacting protein of 76 kDa, also RalBP1) has emerged as a particularly promising target, due both to its cellular and physiological functions which are still being elucidated, and to the marked regression in tumors that has been achieved by blockade of RLIP76 in multiple tumor models (reviewed in(3)). RLIP76 is a multifunctional protein, originally identified as a Ral GTPase effector protein linking Ral to Rho pathways through its RhoGAP activity(4–7). RLIP76 also functions as an ATP-dependent glutathione-conjugate transporter for small molecules, including anticancer drugs and endogenous metabolites(8–10), and in endocytosis(11, 12), mitochondrial fission(13), cell spreading and migration(14). The protein contains binding sites for numerous signaling molecules(4, 5, 14–18); thus, RLIP76 appears to support a scaffolding function to regulate signaling. RLIP76 is expressed in most human tissues including liver, heart, ovary, lung, muscle, and kidney as well as in most human tumor cell lines, and is overexpressed in multiple cancers, such as lung and ovarian carcinomas and melanomas(3, 19–21). Blockade of RLIP76 with targeting antibodies or antisense is associated with increased sensitivity to radiation and chemotherapy and leads to pronounced tumor regression in non-small cell lung and colon carcinomas(22), prostate cancer(23) and B16 melanomas(24) in mice. However, tumor regression in these studies may have resulted from effects in the tumor cells, the animal host cells, or both. Thus, RLIP76 is required for cancer progression and survival but the mechanisms remain unclear.

In this study we investigated a putative role of RLIP76 in neovascularization of solid tumors in mice. For this purpose we refined a new technique of modeling tumor vasculature in 3 dimensions, using X-ray micro-computed tomography(25). Here we present data demonstrating that RLIP76 depletion blocks efficient angiogenesis in tumors, and prevents angiogenesis in Matrigel plugs lacking tumor cells in mice, and we describe correlated defects in endothelial cells in the absence of RLIP76. We propose that RLIP76 regulates tumor progression by modulating survival of the tumor cells themselves as previously demonstrated, as well as supporting neovascularization derived from the host vascular cells.

Materials and Methods

Mice

Generation of RLIP76$^{-/-}$ mice was described previously(26). These mice were backcrossed into the C57Bl/6 background; hence, we used C57Bl/6 wild type mice as isogenic controls. All animal experiments followed protocols approved by the Institutional Animal Care and Use Committee (IACUC) at Temple University.

Cell culture and inoculation of tumor cells *in vivo*

B16F10 mouse melanoma cells and Lewis lung carcinoma (LL/2, LLC) cells were obtained from American Type Culture Collection (ATCC). The cells were cultured in DMEM with 10% FBS in a humidified, 5% CO_2 atmosphere at 37°C. B16F10 and LLC cells were harvested, washed and resuspended at 1×10^6 cells/500 μL of DMEM without serum, and this suspension was injected subcutaneously into the flank of 8-week-old RLIP76$^{-/-}$ or

C57BL/6 mice. Mice were euthanized at 7 or 10 d post-injection. Primary endothelial cells were maintained in EC medium (D/F with 20% FBS, 5% microvascular growth supplement, 0.1% gentamicin/amphotericin B).

Generation of B16F10- and LLC-RLIP76 knockdown cell lines

A plasmid encoding a short hairpin RNA (shRNA) targeting the murine RLIP76 mRNA was generated in pSUPER.retro.puro (OligoEngine) according to the manufacturer's instructions, using the target sequence 5′-GTAGAGAGGACCATGATGT -3′. B16F10 and LLC cells were transfected with the shRNA plasmid or with empty vector using Lipofectamine 2000 (Invitrogen) according to the manufacturer's instructions, and stable transfectants were selected with puromycin. Clones were screened for suppression of RLIP76 expression by western blotting of cell extracts with RLIP76 and α-tubulin antibodies (Santa Cruz Biotechnologies) by standard procedures.

Angiogenesis in Matrigel plugs

The angiogenesis model was based on the use of Matrigel (BD Biosciences) implants in C57BL/6 or RLIP76$^{-/-}$ mice. 500 μL growth factor-reduced Matrigel with or without 100 ng/mL of vascular endothelial growth factor (VEGF) was injected in the mouse flank. After 7 days the mice were euthanized and the Matrigel plugs were dissected away from the tissue, photographed, and then maintained for 24 hours at 4°C. Total hemoglobin levels in the Matrigel plugs were then determined using aqueous extracts as described elsewhere(27). Briefly, a 50 μL aliquot of the extract was removed for analysis. After a 5-minute incubation with 200 μL of DIHB-250 reagent (QuantiChrom hemoglobin assay; BioAssay Systems), hemoglobin content was quantified with a microplate reader at 405 nm.

Endothelial cell isolation

Mice were euthanized, followed by exposure of the thoracic cavity. 10 mL of cold PBS and DMEM was injected via the right ventricle to flush the lungs of blood cells, and then the lungs were subsequently removed and incubated for 60 minutes at 37°C with gentle agitation, with 10 mL of 0.1% collagenase A in a 50-mL centrifuge tube. The tissue/cell suspension was filtered through a 70-μm strainer. The filtered cell suspension was centrifuged for 5 min at 1300 rpm, the cell pellet was washed once with 0.1% BSA/PBS, and then incubated with anti-PECAM-1 (CD31) antibody-conjugated magnetic beads (1×10^7/25 μL, Dynabeads) for 60 min at room temperature. Bead-bound cells were washed 3 times by resuspending in 0.1% BSA/PBS, and separated using a magnet (Invitrogen). Washed cells were resuspended in 1 mL of complete EC media and plated into a 100-mm tissue culture dish coated with a 0.1% collagen, 0.1% amino acid solution. Cells were cultured for 3–7 days before processing.

X-ray micro-computed tomography

A freshly prepared solution of Microfil compound (MV-120, Flow Tech, Inc.) was prepared and used immediately, according to the manufacturer recommendations. The solution consisted of 42% of MV-120, 53% of the diluent solution and 5% of a curing agent. The abdominal cavity and rib cage of each tumor-bearing mouse was opened under anesthesia. Cannulation of the left ventricle was done with a needle connected to a polyethylene catheter while simultaneously nicking the right atrium, and the mouse circulation was perfused with a 0.1% heparinized solution through a pressurized pump. Thereafter 20 mL of the Microfil mixture was perfused through the same catheter(28). The dark blue Microfil suspension readily perfused the peripheral circulation, as within seconds, blood vessels could clearly be seen to fill with the blue Microfil throughout peripheral tissues, including the spleen, colon and other organs, and upon later inspection, blood vessels in the brain were

also perfused (results not shown). The tumor vasculature was also obviously perfused in the LLC tumors, although perfusion of B16 melanomas was difficult to detect due to the dark background of the melanomas themselves (results not shown). The Microfil solution was allowed to polymerize at 4oC overnight, after which the tumors were extracted, fixed in 10% formalin/PBS and scanned in a micro-computed tomography (μCT) unit (Skyscan1172, Skyscan). The X-ray system is based on a microfocus tube reaching a minimum spot size of 3 μm at 8 W, generating projection images irradiating X-ray in cone-beam geometry. Samples were positioned on a computer-controlled rotation stage and scanned 180° around the vertical axis in rotation steps of 0.45°. The samples were operated at a 60 kV peak and 130 μA. Scanned images were processed and analyzed with Analyze 10.0 (AnalyzeDirect) and Skyscan accompanying software.

Migration

EC migration was assessed in modified Boyden chambers. 1×10^4 cells/well were suspended in 250 μL complete EC media. The cells were placed in the top compartment of a standard Boyden chamber with 8 μm membrane pores, coated on the top of the filter with 1 μg/mL collagen, and 500 μL complete EC media was added to the bottom compartment. Chambers were returned to the incubator, and non-migrating ECs were removed from the top compartment with 0.25% trypsin at 3, 6, 9, and 24 hours after adding the cells. ECs cells that had migrated to the bottom compartment were fixed and stained using 0.05% crystal violet. The stained ECs in each well were photographed with the aid of a phase contrast microscope, and mean gray values were determined with Image J.

Proliferation

3-(4,5-dimethylthiazol-2-yl)-2,5-diphenyltetrazolium bromide (MTT) assay was performed to examine EC proliferation(29). Briefly, 1×10^4 ECs were incubated with 12 mM MTT for 3 hours at 37°C. The amount of MTT formazan product was determined by measuring absorbance at 570 nm using a microplate reader.

In vitro cord formation assay

80 μL of growth factor-containing Matrigel was added to each well of a 24-well tissue culture plate, and the plates were incubated at 37°C for 30 min to solidify the gel. 1×10^5 primary endothelial cells were seeded in each well in 100 μL of growth medium. After 3, 6, and 9 hours, the center of each well was photographed under a microscope. Branch numbers were counted as branches per each field at 9 hours (n=3).

Animal model for two-stage phorbol ester (PMA) carcinogenesis

Phorbol 12-myristate 13-acetate (PMA) and 7,12-dimethyl-benz[a]anthracene (DMBA) were from Sigma. RLIP76 as well as scrambled antisense were purchased from Biosynthesis, Inc.(24). Control as well as RLIP76 proteoliposomes were prepared using established procedures as described previously(6). Avidin/biotin complex (ABC) detection kits were purchased from Vector. Skin carcinogenesis experiments were performed as described previously(30). Briefly, thirty-two (16 WT and 16 $RLIP76^{-/-}$) 12-week-old mice were divided into 4 groups of 8 animals. The backs of the mice were shaved with electric clippers and the treatment was applied by a cotton applicator to a 1 cm^2 shaved area of skin on the animal's back. Treatments were as follows: **Group # 1**, $RLIP76^{+/+}$ mice treated first with DMBA (25 nmol in 0.1 mL acetone) followed two weeks later by 200 μg/0.2 mL scrambled antisense, i.p., then PMA (10 nmol in 0.1 mL acetone single dose) treatment 24 h after the antisense treatment; **Group # 2**, $RLIP76^{+/+}$ mice treated first with DMBA and followed two weeks later by 200 μg/0.2 mL RLIP76 antisense, i.p., then PMA treatment 24 h after the RLIP76 antisense treatment; **Group # 3**, $RLIP76^{-/-}$ mice treated first with

DMBA and followed two weeks later by 0.2 mL control liposomes, i.p., and then PMA treatment 24 h after the liposomes treatment; **Group # 4**, RLIP76$^{-/-}$ mice treated first with DMBA and followed two weeks later by 200 μg/0.2 mL RLIP76 liposomes, i.p., and then PMA treatment 24 h after the RLIP76 liposomes treatment. Skin from all the groups was harvested 4 days later and prepared for histopathologic analyses with anti-CD31 (Invitrogen) and anti-Ki67 antibodies (Santa Cruz Biotechnology) and Universal ABC detection kit as described below.

Hematoxylin and eosin staining of tumor sections

Sections of paraffin-embedded B16F10 and LLC tumors were immersed in xylene for 5 min to dissolve the paraffin and then rehydrated. Subsets of sections were then stained with hematoxylin and eosin (H&E). Sections were stained in Biebrich scarlet-acid fuchsin solution for 15 min and then rinsed in ddH_2O. Sections were incubated in phosphomolybdic-phosphotungstic acid solution for 15 min and then transferred directly (without rinse) to aniline blue solution and stained for 5–10 min. Sections were then rinsed in ddH_2O and washed in 1% acetic acid solution for 2–5 min and then rinsed in ddH_2O. Stained sections were dehydrated, mounted under coverslips with DPX as a mounting medium, and observed using a Nikon-Eclipse E300 light microscope (10x objective lens; n.a. = 0.3) connected to a Nikon Digital Sight camera. Images were captured and processed using NIS-Elements F3.0 software.

Immunohistochemistry

B16F10 and LLC primary tumors from 8-week-old RLIP76$^{-/-}$ and C57BL/6 mice were harvested, fixed in 3.7% paraformaldehyde, embedded in paraffin, and sectioned into 5μm horizontal sections. Sections were dried overnight at room temperature (RT) after placement onto charged slides. Sections were then immersed in 100% xylene for 3 min to dissolve the paraffin, and then rehydrated through graded ethanol to ddH_2O. Sections were incubated with 3% hydrogen peroxide for 20 h to inhibit endogenous peroxidase activity, rinsed in ddH_2O, and then incubated with 0.4% pepsin for 20 min. Sections were incubated with bovine serum (1% serum in phosphate buffer) for 1 h, and then primary antibodies were added at a dilution of 1:500 in the blocking serum overnight at 4oC. The next day, sections were washed in PBS four times on a shaker, then fluorescein-conjugated secondary antibodies were applied at a dilution of 1:1000 for 1 h at RT. Fluorescent-stained sections were washed with PBS, and then incubated with DAPI, mounted under coverslips with 80% glycerol/PBS, and observed using a Nikon-Eclipse E1000 epifluorescent microscope (20x objective lens; n.a. = 0.75) connected to a Q Imaging RETIGA EXi camera.

Statistical analysis

One-way ANOVA followed by Fisher PLSD analysis was used for all statistical data analysis, using StatView (SAS). A 5% probability was considered significant.

Results and Discussion

We established a model of tumor formation and growth in RLIP76 knock-out ($^{-/-}$)(26) and wild type (WT) isogenic C57BL/6 mice, xenografted with B16F10 melanoma cells or Lewis lung carcinoma (LLC) cells, injected as a bolus into the mouse flanks. After 7 days the tumors were removed for morphometric and histological analyses. Although discreet, dense neoplasias grew rapidly at the site of injection in all cases, solid tumors of both types were significantly smaller in RLIP76$^{-/-}$ mice than in the wild type mice (Fig. 1). Tumor regression in earlier studies with RLIP76 antisense or antibodies may have resulted from effects in the tumor cells, the animal host cells, or both. In the present study RLIP76 was expressed in the tumor cells, suggesting that the inhibition of tumor growth we observed in

RLIP76$^{-/-}$ mice was primarily due to blockade of a RLIP76-dependent response in the animal host. To address this possibility, we generated B16F10 and LLC cell lines in which endogenous RLIP76 expression is constitutively knocked down by expression of a stably incorporated targeting short hairpin RNA (shRNA) (Suppl. Fig. 1). When implanted into mice, the RLIP76 knockdown cells produced tumors that were slightly smaller than their normal cell counterparts in either WT or RLIP76$^{-/-}$ mice, but as before the tumors were significantly smaller in RLIP76$^{-/-}$ compared to WT mice for each case (Fig. 1b). Together these data suggested a strong host-dependent role of RLIP76 in tumor growth. Therefore we considered that neovascularization of the tumors, essential for tumor progression, may be impaired in RLIP76$^{-/-}$ mice.

Inspection of histological sections revealed the presence of large and small blood vessels in the tumors xenografted in the WT mice. Sections from tumors derived in RLIP76$^{-/-}$ mice also contained blood vessels, although there appeared to be fewer large vessels and the overall vascular density appeared diminished compared to WT, suggesting diminished neovascularization in tumors in the RLIP76$^{-/-}$ mice (Suppl. Fig. 2). However, such 2D snapshots provide an incomplete picture of the tumor vasculature and can introduce artifacts(31). We adapted X-ray micro-computed tomography (μCT) to reproduce and subsequently analyze the competent vasculature in 3D in tumors derived in these mice(32). In order to visualize competent blood vessels and to resolve them from surrounding tumor tissue by X-ray scanning, we perfused the peripheral blood circulation in the mice through a needle inserted in the left ventricle of the heart, attached by tubing to a perfusion pump, first with heparin to prevent coagulation followed by Microfil. Microfil is a silicon-based, electron-dense suspension with sufficiently limited viscosity to perfuse blood vessels down to small diameter capillaries, after which the Microfil hardens to form a cast of the vascular lumenal space connected to the peripheral circulation(28). We applied this technique to form vascular casts within the tumors 7 days after injection of tumor cells. We extracted the tumors after Microfil perfusion and scanned them by X-ray μCT to visualize the tumor vasculature.

The X-ray μCT scanning allowed us to reconstruct 3D models of the vasculature in the tumors by computer-assisted assembly of 3D structures from several thousand 2D X-ray scans per sample (Fig. 2a and Suppl. Movies 1–4). These reconstructions offered new views of the vasculature in the xenografted tumors that could not be appreciated from histological analysis of 2D sections. Branched vascular networks could be seen in both LLC and B16F10 tumors derived in WT and RLIP76$^{-/-}$ mice, in all cases apparently based around a single major vessel in the center of the tumor mass from which smaller vessels had branched. Thus, the Microfil perfusion coupled with X-ray μCT scanning reproduced 3D constructions of intact tumor vasculature. The substantial degree of angiogenesis in the nascent tumors at only 7 d post-injection was somewhat surprising, even given the aggressive nature of both cancer types(33, 34); however, clear differences between tumors in WT and RLIP76$^{-/-}$mice were readily apparent. Gross observations indicated that a generally more advanced stage of angiogenesis had been reached in the tumors xenografted in WT mice. The central vessels appeared thicker and longer than those in the RLIP76$^{-/-}$ mice, with many branching vessels of various thicknesses. In contrast, the central vessels in the tumors in the RLIP76$^{-/-}$ mice appeared narrower and shorter, and branching vessels also appeared thinner and shorter than in the WT (Fig. 2a). A significant advantage of the μCT analysis is that it allows for comprehensive quantification of vascular geometries in three dimensions. Thus, from these 3D reconstructions we determined that the total vascular volume within tumors derived in RLIP76$^{-/-}$ mice was significantly less than that of tumors derived in WT mice (results not shown, see Fig. 2b). To ensure that the blockade in tumor angiogenesis in RLIP76$^{-/-}$ mice was not solely a consequence of smaller overall tumor volumes in these mice, we determined total vascular volumes in tumors of the same size (WT, 7 d; RLIP76$^{-/-}$, 10 d)

and found that angiogenesis was still markedly blocked in tumors in the RLIP76$^{-/-}$ mice compared to those from WT mice (Fig. 2b). Similarly, CD31 staining of paraffin sections derived from these tumors showed extensive angiogenesis in wild type mice (at 7 d), in contrast to RLIP76$^{-/-}$ mice (at 10 d), from which the tumor sections showed sparse CD31 staining mostly concentrated in smaller vessels (Suppl. Fig. 3).

Consistent with these results, small diameter vessels (notably in the range of 3–14μm) made up a higher percentage of the total individual vessels in both tumor types in RLIP76$^{-/-}$ mice than in WT mice (Fig. 2c). The smaller diameters of blood vessels in the RLIP76$^{-/-}$-derived tumors correlated with diminished individual vessel volumes (and thus, indicative of shorter vessel lengths) compared to WT-derived tumors, which showed a range of vessel diameters including many vessels with diameters > 100 μm; some of these wide diameter vessels were $> 5 \times 10^8 \mu m^3$ in volume (Fig. 2d). Thus, targeted depletion of RLIP76 in mice prevented efficient neovascularization in implanted solid tumors. This blockade effect was due to diminished vessel growth and maturation in the absence of RLIP76. These results further highlight the value of X-ray μCT for comprehensive analysis of whole vascular structures in solid tumors *in vivo*.

The above results showed that angiogenesis was blocked in the implanted tumors in mice depleted of RLIP76; however, the tumor cells expressed RLIP76 in this system, and RLIP76 blockade has widespread anti-tumor effects(3). To assess the relationship between the anti-tumor effects of RLIP76 inhibition and its roles in tumor angiogenesis, we measured vascular volumes in tumors derived from RLIP76-knockdown cells. Angiogenic vascular volumes in these tumors were slightly diminished overall from those seen in tumors derived from the non-knockdown cells, but displayed similar ratios comparing RLIP76$^{-/-}$ to WT mice in each case, i.e., significantly diminished vascular volumes in RLIP76$^{-/-}$ mice compared to WT (Suppl. Fig. 4, cf. Fig. 2b). Thus, RLIP76 contributes independently to growth of tumor cells and to angiogenesis from the host vasculature in solid tumors, such that combined depletion in both compartments further reduces tumor growth and tumor angiogenesis over those observed by knockout in the host animal only. The added effects of knockdown in the tumor cells on overall tumor growth were minimal; however, residual effects of low levels of RLIP76 expression in these cells could not be ruled out.

We next considered whether angiogenesis would be blocked in RLIP76$^{-/-}$ mice in the case of induced tumorigenesis, using a model of spontaneous skin carcinogenesis after treatment with DMBA (tumor initiator) followed by PMA (tumor promoter). We have previously shown that these mice are strongly resistant to chemical neoplasia in response to these agents; hence, the induced tumors were much smaller in these mice than in WT mice(30). Paraffin sections of the treated areas in RLIP76$^{-/-}$ mice showed significantly diminished staining for Ki67, a proliferation marker, in contrast to robust proliferation in treated areas in WT mice. CD31 staining was minimal in these sections from RLIP76$^{-/-}$ mice, whereas chemically-induced tumors showed strong staining for CD31 in WT mice (Suppl. Fig. 5). Thus, RLIP76 depletion blocked angiogenesis in a model of spontaneous chemical carcinogenesis in mice. Moreover, depletion of RLIP76 in induced skin tumors in WT mice by treatment with RLIP76 antisense suppressed skin carcinogenesis in this model, as we have previously observed(30), and also blocked angiogenesis as indicated by minimal CD31 staining in these sections. Conversely, topical liposome-mediated application of RLIP76 protein(26) in RLIP76$^{-/-}$ mice restored both chemical carcinogenesis (Ki67) and angiogenesis (CD31) in the induced tumors (Suppl. Fig. 5). Thus, RLIP76 is necessary for angiogenesis in chemically induced carcinogenesis in mice.

Based on the above results, we considered whether RLIP76 depletion is associated with a general defect in angiogenic responses, in the absence of tumors. To investigate this

possibility, we assessed angiogenesis in growth factor-depleted Matrigel plugs containing 100 ng/mL VEGF as an added angiogenic stimulant. Matrigel plugs with or without VEGF were removed 7 d after implantation. Matrigel plugs from WT mice appeared blood-filled, indicating robust angiogenesis (Fig. 3a), and this effect was enhanced slightly but significantly by infusion of the plug with VEGF (Fig. 3b). In sharp contrast, Matrigel plugs implanted in RLIP76$^{-/-}$ mice with or without VEGF were completely devoid of blood and blood vessels (Fig. 3). Thus, RLIP76 is required for angiogenesis in Matrigel *in vivo*.

To investigate the cellular mechanisms of suppressed tumor angiogenesis in RLIP76$^{-/-}$ mice, we isolated microvascular endothelial cells (ECs) from wild type and RLIP76$^{-/-}$ mice, and analyzed functions of these cells *in vitro*. Migration through collagen-coated filters was substantially impaired in the RLIP76$^{-/-}$ endothelial cells compared to WT (Fig. 4a). Moreover, RLIP76$^{-/-}$ ECs grown in culture proliferated at a slower rate than WT ECs (Fig. 4b). As an *in vitro* approximation of angiogenesis we assessed cord formation by ECs seeded on Matrigel-coated surfaces. Whereas WT cells rapidly coalesced to form anastomosed networks, this response was greatly diminished in RLIP76$^{-/-}$ ECs (Fig. 4c). Although the RLIP76$^{-/-}$ cells aggregated partially in small clusters, these clusters did not form coherent networks as indicated by a marked diminution in branch points after 9 h in Matrigel (Fig. 4d). Together these data indicate that RLIP76 is necessary for efficient endothelial cell migration, proliferation, and cord formation *in vitro*. Antibodies targeting RLIP76 have been shown to induce apoptosis in these cells; hence, RLIP76 is also important for endothelial cell survival(35). These diminished endothelial cell responses in the absence of RLIP76 correlated with decreased angiogenesis in RLIP76$^{-/-}$ mice, and suggest that the angiogenesis defects in RLIP76$^{-/-}$ mice were due substantially to defects in endothelial cell functions. However, as RLIP76 is globally deleted in these mice, RLIP76-dependent functions in other cells may also contribute to the angiogenesis defect and reduction in tumor growth.

In this study we identified and characterized new physiological and pathophysiological roles for RLIP76: angiogenesis, and neovascularization of solid tumors. These results substantiate earlier findings that RLIP76 is required for tumor growth and tumor cell survival(3), and expand our understanding of the contributions of RLIP76 to cancer. Together these results indicate a dual requirement for RLIP76: for survival of the tumor cells themselves, and for angiogenesis from the host, necessary for cancer progression. The former has been correlated with glutathione transport function(36), but may also be due to other functions such as its role in mitochondrial fission(13). Similarly, RLIP76 interacts in cells with the small GTPase R-Ras to regulate cell motility(14); however, R-Ras has been described as an angiogenesis inhibitor(37, 38) whereas RLIP76 is required for angiogenesis. Alternatively, RLIP76 regulation of endocytosis(11, 12, 39) or actin dynamics(40), mediated in part by interaction with Ral GTPase, may also play prominent roles in its effects on angiogenesis. Thus, the relationships between the cellular and molecular functions of RLIP76 and its roles in cancer progression and angiogenesis remain to be fully explained but are likely to be manifold. We anticipate that approaches such as X-ray μCT will be valuable in uncovering the roles of RLIP76 and other proteins in vascular pathologies and cancer.

Supplementary Material

Refer to Web version on PubMed Central for supplementary material.

Acknowledgments

We thank Robin Pixley and Mary Barbe for technical assistance with X-ray micro-computed tomography, and Roshanak Razmpour for assistance with histology.

Grant Support

This work was supported by NIH grant HL093416 to LG and USPHS grant CA77495 to SA and SS.

References

1. Folkman J. The role of angiogenesis in tumor growth. Semin Cancer Biol. 1992; 3:65–71. [PubMed: 1378311]
2. Adams RH, Alitalo K. Molecular regulation of angiogenesis and lymphangiogenesis. Nat Rev Mol Cell Biol. 2007; 8:464–78. [PubMed: 17522591]
3. Awasthi S, Singhal SS, Awasthi YC, Martin B, Woo JH, Cunningham CC, et al. RLIP76 and Cancer. Clin Cancer Res. 2008; 14:4372–7. [PubMed: 18628450]
4. Jullien-Flores V, Dorseuil O, Romero F, Letourneur F, Saragosti S, Berger R, et al. Bridging Ral GTPase to Rho pathways. RLIP76, a Ral effector with CDC42/Rac GTPase-activating protein activity. Journal of Biological Chemistry. 1995; 270:22473–7. [PubMed: 7673236]
5. Cantor SB, Urano T, Feig LA. Identification and characterization of Ral-binding protein 1, a potential downstream target of Ral GTPases. MolCell Biol. 1995; 15:4578–84.
6. Awasthi S, Cheng J, Singhal SS, Saini MK, Pandya U, Pikula S, et al. Novel function of human RLIP76: ATP-dependent transport of glutathione conjugates and doxorubicin. Biochemistry. 2000; 39:9327–34. [PubMed: 10924126]
7. Park SH, Weinberg RA. A putative effector of Ral has homology to Rho/Rac GTPase activating proteins. Oncogene. 1995; 11:2349–55. [PubMed: 8570186]
8. Awasthi S, Cheng JZ, Singhal SS, Pandya U, Sharma R, Singh SV, et al. Functional reassembly of ATP-dependent xenobiotic transport by the N- and C-terminal domains of RLIP76 and identification of ATP binding sequences. Biochemistry. 2001; 40:4159–68. [PubMed: 11300797]
9. Awasthi S, Sharma R, Yang Y, Singhal SS, Pikula S, Bandorowicz-Pikula J, et al. Transport functions and physiological significance of 76 kDa Ral-binding GTPase activating protein (RLIP76). Acta Biochim Pol. 2002; 49:855–67. [PubMed: 12545192]
10. Awasthi S, Singhal SS, Sharma R, Zimniak P, Awasthi YC. Transport of glutathione conjugates and chemotherapeutic drugs by RLIP76 (RALBP1): a novel link between G-protein and tyrosine kinase signaling and drug resistance. IntJCancer. 2003; 106:635–46.
11. Nakashima S, Morinaka K, Koyama S, Ikeda M, Kishida M, Okawa K, et al. Small G protein Ral and its downstream molecules regulate endocytosis of EGF and insulin receptors. EMBO Journal. 1999; 18:3629–42. [PubMed: 10393179]
12. Rosse C, L'Hoste S, Offner N, Picard A, Camonis J. RLIP, an effector of the Ral GTPases, is a platform for Cdk1 to phosphorylate epsin during the switch off of endocytosis in mitosis. Journal of Biological Chemistry. 2003; 278:30597–604. [PubMed: 12775724]
13. Kashatus DF, Lim KH, Brady DC, Pershing NL, Cox AD, Counter CM. RALA and RALBP1 regulate mitochondrial fission at mitosis. Nat Cell Biol. 2011; 13:1108–15. [PubMed: 21822277]
14. Goldfinger LE, Ptak C, Jeffery ED, Shabanowitz J, Hunt DF, Ginsberg MH. RLIP76 (RalBP1) is an R-Ras effector that mediates adhesion-dependent Rac activation and cell migration. Journal of Cell Biology. 2006; 174:877–88. [PubMed: 16966426]
15. Hu Y, Mivechi NF. HSF-1 interacts with Ral-binding protein 1 in a stress-responsive, multiprotein complex with HSP90 in vivo. Journal of Biological Chemistry. 2003; 278:17299–306. [PubMed: 12621024]
16. Ikeda M, Ishida O, Hinoi T, Kishida S, Kikuchi A. Identification and characterization of a novel protein interacting with Ral-binding protein 1, a putative effector protein of Ral. Journal of Biological Chemistry. 1998; 273:814–21. [PubMed: 9422736]
17. Yamaguchi A, Urano T, Goi T, Feig LA. An Eps homology (EH) domain protein that binds to the Ral-GTPase target, RalBP1. Journal of Biological Chemistry. 1997; 272:31230–4. [PubMed: 9395447]
18. Jullien-Flores V, Mahe Y, Mirey G, Leprince C, Meunier-Bisceuil B, Sorkin A, et al. RLIP76, an effector of the GTPase Ral, interacts with the AP2 complex: involvement of the Ral pathway in receptor endocytosis. Journal of Cell Science. 2000; 113 (Pt 16):2837–44. [PubMed: 10910768]

19. Sharma R, Gupta S, Singh SV, Medh RD, Ahmad H, LaBelle EF, et al. Purification and characterization of dinitrophenylglutathione ATPase of human erythrocytes and its expression in other tissues. Biochem Biophys Res Commun. 1990; 171:155–61. [PubMed: 2144112]
20. Awasthi S, Singhal SS, Srivastava SK, Zimniak P, Bajpai KK, Saxena M, et al. Adenosine triphosphate-dependent transport of doxorubicin, daunomycin, and vinblastine in human tissues by a mechanism distinct from the P-glycoprotein. J Clin Invest. 1994; 93:958–65. [PubMed: 7907606]
21. Awasthi YC, Singhal SS, Gupta S, Ahmad H, Zimniak P, Radominska A, et al. Purification and characterization of an ATPase from human liver which catalyzes ATP hydrolysis in the presence of the conjugates of bilirubin bile acids and glutathione. Biochem Biophys Res Commun. 1991; 175:1090–6. [PubMed: 1827256]
22. Singhal SS, Singhal J, Yadav S, Dwivedi S, Boor PJ, Awasthi YC, et al. Regression of lung and colon cancer xenografts by depleting or inhibiting RLIP76 (Ral-binding protein 1). Cancer Res. 2007; 67:4382–9. [PubMed: 17483352]
23. Singhal SS, Roth C, Leake K, Singhal J, Yadav S, Awasthi S. Regression of prostate cancer xenografts by RLIP76 depletion. Biochem Pharmacol. 2009; 77:1074–83. [PubMed: 19073149]
24. Singhal SS, Awasthi YC, Awasthi S. Regression of melanoma in a murine model by RLIP76 depletion. Cancer Res. 2006; 66:2354–60. [PubMed: 16489041]
25. Schambach SJ, Bag S, Schilling L, Groden C, Brockmann MA. Application of micro-CT in small animal imaging. Methods. 2009; 50:2–13. [PubMed: 19706326]
26. Awasthi S, Singhal SS, Yadav S, Singhal J, Drake K, Nadkar A, et al. RLIP76 is a major determinant of radiation sensitivity. Cancer Res. 2005; 65:6022–8. [PubMed: 16024601]
27. Lucidarme O, Nguyen T, Kono Y, Corbeil J, Choi SH, Varner J, et al. Angiogenesis model for ultrasound contrast research: exploratory study. Acad Radiol. 2004; 11:4–12. [PubMed: 14746396]
28. Grabherr S, Hess A, Karolczak M, Thali MJ, Friess SD, Kalender WA, et al. Angiofil-mediated visualization of the vascular system by microcomputed tomography: a feasibility study. Microsc Res Tech. 2008; 71:551–6. [PubMed: 18393302]
29. Garn H, Krause H, Enzmann V, Drossler K. An improved MTT assay using the electron-coupling agent menadione. J Immunol Methods. 1994; 168:253–6. [PubMed: 8308299]
30. Singhal SS, Wickramarachchi D, Yadav S, Singhal J, Leake K, Vatsyayan R, et al. Glutathione-conjugate transport by RLIP76 is required for clathrin-dependent endocytosis and chemical carcinogenesis. Mol Cancer Ther. 2011; 10:16–28. [PubMed: 21220488]
31. Fox SB. Assessing tumor angiogenesis in histological samples. Methods Mol Biol. 2009; 467:55–78. [PubMed: 19301664]
32. Savai R, Langheinrich AC, Schermuly RT, Pullamsetti SS, Dumitrascu R, Traupe H, et al. Evaluation of angiogenesis using micro-computed tomography in a xenograft mouse model of lung cancer. Neoplasia. 2009; 11:48–56. [PubMed: 19107231]
33. Fidler IJ. Biological behavior of malignant melanoma cells correlated to their survival in vivo. Cancer Res. 1975; 35:218–24. [PubMed: 1109790]
34. Bertram JS, Janik P. Establishment of a cloned line of Lewis Lung Carcinoma cells adapted to cell culture. Cancer Lett. 1980; 11:63–73. [PubMed: 7226139]
35. Margutti P, Matarrese P, Conti F, Colasanti T, Delunardo F, Capozzi A, et al. Autoantibodies to the C-terminal subunit of RLIP76 induce oxidative stress and endothelial cell apoptosis in immune-mediated vascular diseases and atherosclerosis. Blood. 2008; 111:4559–70. [PubMed: 17993611]
36. Singhal SS, Sehrawat A, Mehta A, Sahu M, Awasthi S. Functional reconstitution of RLIP76 catalyzing ATP-dependent transport of glutathione-conjugates. Int J Oncol. 2009; 34:191–9. [PubMed: 19082490]
37. Komatsu M, Ruoslahti E. R-Ras is a global regulator of vascular regeneration that suppresses intimal hyperplasia and tumor angiogenesis. Nat Med. 2005; 11:1346–50. [PubMed: 16286923]
38. Inuzuka T, Tsuda M, Kawaguchi H, Ohba Y. Transcription factor 8 activates R-Ras to regulate angiogenesis. Biochem Biophys Res Commun. 2008

39. Santambrogio M, Valdembri D, Serini G. Increasing traffic on vascular routes. Mol Aspects Med. 2011; 32:112–22. [PubMed: 21536065]

40. Lebreton S, Boissel L, Iouzalen N, Moreau J. RLIP mediates downstream signalling from RalB to the actin cytoskeleton during Xenopus early development. MechDev. 2004; 121:1481–94.

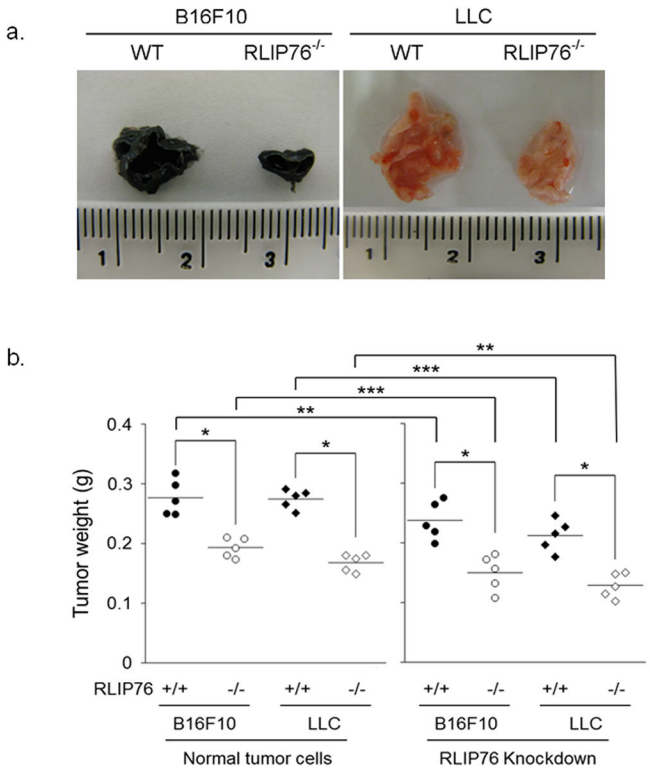

Figure 1. Primary solid tumor growth is inhibited in RLIP76$^{-/-}$ mice

(a) Macroscopic appearance of 7-day-old B16F10 melanomas (left) and LLC carcinomas (right) derived from a bolus injection of 1×10^6 tumor cells in the flanks of wild type (WT) and RLIP76$^{-/-}$ mice. (b) Dry mass of B16F10 (left) and LLC (right) tumors from wild type ($^{+/+}$) and RLIP76$^{-/-}$ ($^{-/-}$) mice (n=5 each). Left panels, Normal (non-knockdown) tumor cells; right panels, RLIP76 knockdown tumor cells. (* $p < 0.001$, ** $p < 0.015$, *** $p < 0.008$). Average dry mass of B16F10 tumors: WT 0.277 g ± 0.013; RLIP76$^{-/-}$0.193 g ± 0.007; LLC tumors: WT 0.274 g ± 0.007, RLIP76$^{-/-}$ 0.168 g ± 0.007. Average masses of RLIP76 knockdown tumors, B16F10: WT 0.238 g ± 0.014; RLIP76$^{-/-}$ 0.150 g ± 0.013; RLIP76 knockdown tumors, LLC: WT 0.212 g ± 0.012, RLIP76$^{-/-}$ 0.128 g ± 0.009. Results are shown ± s.e.m.

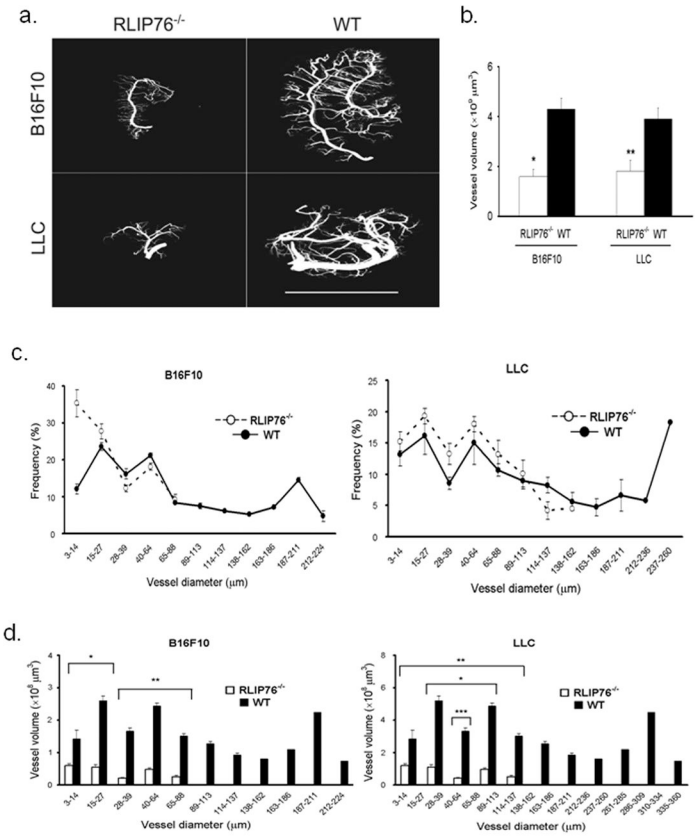

Figure 2. Tumor neovascularization is inhibited in RLIP76$^{-/-}$ mice

(a) Images of B16F10 (top) and LLC (bottom) acquired by X-ray μCT scanning and 3D reconstruction of tumors perfused through the peripheral blood circulation with Microfil in RLIP76$^{-/-}$ and wild type (WT) mice. Bar, 10 mm. (b) Total vessel volumes were determined using μCT 3D reconstructed images from tumors derived in RLIP76$^{-/-}$ (white bars) and WT (black bars) mice. B16F10, left; LLC, right. Average total vessel volumes (x $10^9\mu m^3$) of B16F10 tumors: WT 4.3 ± 0.44; RLIP76$^{-/-}$ 1.6 ± 0.29; LLC tumors: WT 3.9 ± 0.44, RLIP76$^{-/-}$ 1.8 ± 0.42. (n=3 each) (* $p < 0.01$, **, $p < 0.001$). (c) Frequency distribution of the vascular diameters in B16F10 (left) and LLC (right) tumors in RLIP76$^{-/-}$ (○) and WT mice (●). (d) Individual vessel volumes plotted against vascular diameters in B16F10 (left, * $p < 0.003$, ** $p < 0.05$) and LLC (right, * $p < 0.001$, ** $p < 0.001$, *** $p < 0.005$) tumors derived in RLIP76$^{-/-}$ (white bars) and WT (black bars) mice. Results are shown ± s.e.m.

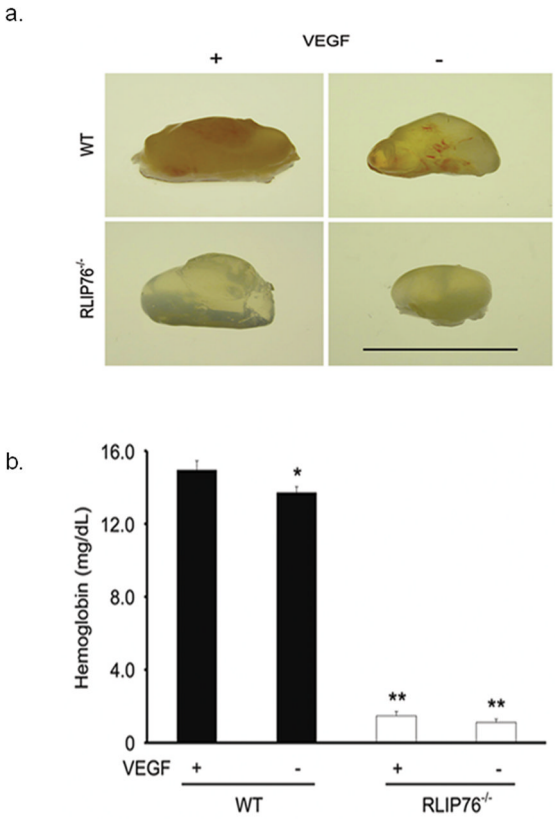

Figure 3. Angiogenesis in Matrigel plugs is inhibited in RLIP76$^{-/-}$ mice

(a) Matrigel plugs with (+) or without (−) vascular endothelial growth factor (VEGF, 100 ng/mL) in wild type (WT, top) and RLIP76$^{-/-}$ (bottom) mice. Bar, 1 cm. (b) Hemoglobin concentration in Matrigel plugs in WT (black bars) and RLIP76$^{-/-}$ (white bars) mice (n=3 each). * $p < 0.03$, ** $p < 0.0001$. Results are shown + s.e.m.

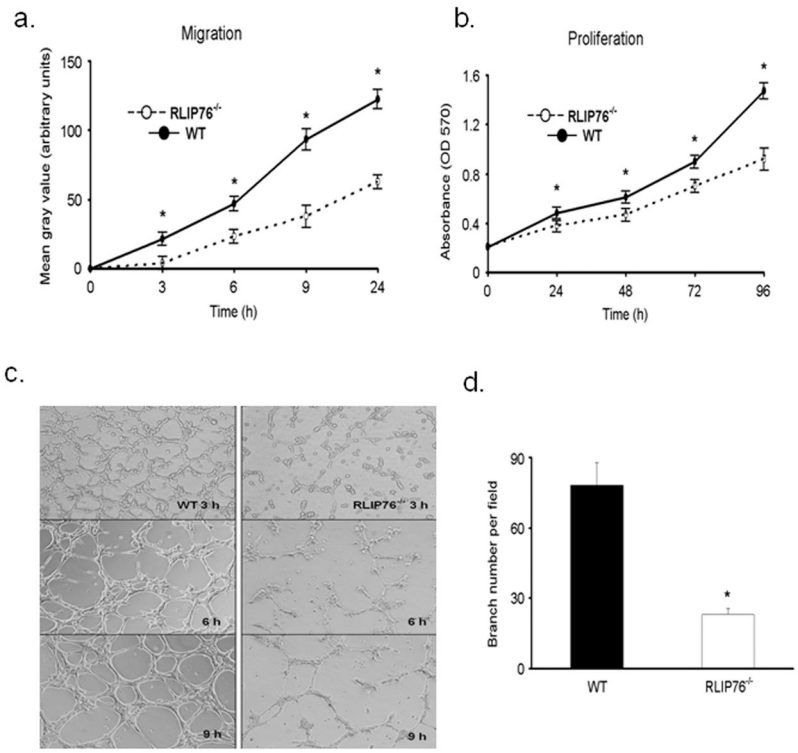

Figure 4. Migration, proliferation, and anastomosing cord formation are defective in RLIP76$^{-/-}$endothelial cells (ECs)

(a) Migration of wild type (WT, ●) and RLIP76$^{-/-}$ (○) ECs through collagen-coated filters in modified Boyden chambers. At the indicated times after seeding cells on the tops of the filters, the undersides of the filters were fixed and stained with crystal violet solution. Staining intensities, indicating densities of migrated cells in duplicate wells from three independent experiments are shown ± s.e.m. * $p < 0.0001$. (b) Proliferation rates of WT and RLIP76$^{-/-}$ ECs *in vitro* measured by MTT assay are shown ± s.e.m. n=3 independent experiments with duplicate wells per sample. * $p < 0.0001$. (c) Matrigel cord formation by WT and RLIP76$^{-/-}$ ECs. 1×10^5 WT (left) or RLIP76$^{-/-}$ (right) ECs seeded in Matrigel-coated wells were imaged at the indicated times (n=3). (d) Average branch points from (c) at 9 h in Matrigel for WT (black bar) and RLIP76$^{-/-}$ (white bar) ECs are shown ± s.e.m. * $p < 0.005$.